A Novel Approach to Utilize PLC to Detect Corroded and Eroded Segments of Power Transmission Lines

R. Jalilzadeh Hamidi, *Student Member, IEEE*,
Seyed Hossein Hosseinian, Seyed Hossein Hesamedin Sadeghi, *Senior Member, IEEE*,
and Zhihua Qu, *Fellow, IEEE*

***Abstract*—A great number of existing power transmission lines have aged throughout the world. A considerable proportion of them are located in the environments that exacerbate their corrosion and erosion process. In-time detection of defects necessitates the use of nondestructive testing (NDT) techniques. Scanning the lines with robots and helicopters are the methods in use. In this paper, we propose a new NDT technique that uses the elements of power-line carriers, generally for information communication purposes, to detect the possibly corroded and eroded segments of each phase along a transmission line. The proposed NDT technique is based on the backward-wave propagation produced by a change in the characteristic impedance of a power transmission line, resulting from corrosion and erosion. To demonstrate the viability of the proposed approach, "EMTPWorks" is used to perform simulations. It is shown that the proposed technique can locate the surface defects and estimate the severity of them in transmission line conductors.**

***Index Terms*—Conductor aging, corrosion, erosion, nondestructive testing (NDT), power-line carrier (PLC).**

I. Introduction

CORROSIVE contaminants, present in the atmosphere, decrease the lifetime of overhead transmission line conductors. The importance of the atmosphere as a corrosive agent is confirmed by a number of scientific publications [1], [2]. The corrosive action of the atmosphere depends on several factors, including relative humidity, pollutant substances, temperature, and the stay time of an electrolyte film on a metallic surface. In addition, climatic eroding factors, such as wind direction, wind intensity, rainfall, and solar radiation could undermine the structural integrity of transmission line conductors. Internal corrosion is a major factor that limits the life of aluminum conductor steel-reinforced (ACSR) conductors, but corrosive pollutants and erosion damage the outer strands of any conductor type.

Manuscript received May 17, 2011; revised April 07, 2012; accepted May 05, 2014. Date of publication February 13, 2015; date of current version March 20, 2015. Paper no. TPWRD-00414-2011.

R. J. Hamidi, S. H. Hosseinian, and S. H. H. Sadeghi are with the Electrical Engineering Department, Amirkabir University of Technology, Tehran 15914, Iran (e-mail: reza.j.hamidi@aut.ac.ir; hosseinian@aut.ac.ir; sadeghi@aut.ac.ir).

Z. Qu is with the Electrical and Computer Engineering Department, University of Central Florida, Orlando, FL 32816-2362 USA (e-mail: qu@eecs.ucf.edu).

Color versions of one or more of the figures in this paper are available online at http://ieeexplore.ieee.org.

Digital Object Identifier 10.1109/TPWRD.2014.2326167

Early warning of damage enables operators to make the best use of the budget for reconductoring an aging network. The major consequences of decreased reliability of aged lines are a reduction in system operability, maintainability, supply reliability, and public safety [3]–[6].

The scope of this paper is to nondestructively detect surface flaws in transmission line conductors.

The NDT techniques that are commonly used in the industry include line scanning with robots [6], [8] or helicopters [9], [10] using visual and corona cameras, or ultrasonic probes. These methods need close contact with the conductors, thus making them expensive and unsafe for repair teams.

It is common in NDT&E procedures that the test specimen is exposed to an interrogatory wave, and the reflected wave is employed to estimate the condition of the specimen. A power-line carrier (PLC) is able to generate and receive a range of frequencies from 30–40 kHz to 500 kHz [7]. Fortunately, PLCs are usually installed in substations, especially in high-voltage (HV) and ultra-high voltage (UHV) sections where they almost always exist. Therefore, we addressed the application of PLCs to find defects in transmission lines.

According to the results, the proposed NDT&E technique is able to approximately detect the flaws in the outer strands of the conductors. The results also show that the proposed method is capable of finding either single or multiple defects in each phase, whether the other phases are intact or damaged. The information provided by the method would decrease the cost and increase the safety of the maintenance procedure.

II. Conductors and Wave Propagation

The most common conductor type is ACSR. The features of the conductors used in the current study are presented in Table I. An infinitely small section of one phase of a long line is shown in Fig. 1. With reference to Fig. 1, the transmission line equations are stated in (1)–(4) from [11]

$$-\frac{\partial u(x,t)}{\partial x} = R' i(x,t) + L' \frac{\partial i(x,t)}{\partial t} \tag{1}$$

$$-\frac{\partial i(x,t)}{\partial x} = G' u(x,t) + C' \frac{\partial u(x,t)}{\partial t} \tag{2}$$

$$Z_C = \sqrt{\frac{(R' + j\omega L')}{(G' + j\omega C')}} \tag{3}$$

$$\gamma = \sqrt{(R' + j\omega L')(G' + j\omega C')} \tag{4}$$

where R', L', C', and G' are variables per length unit.

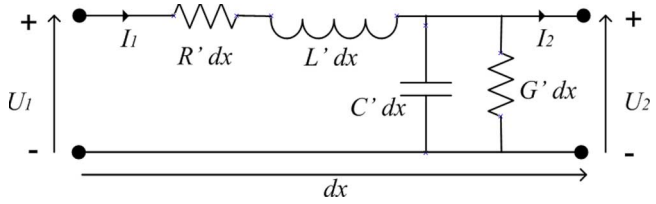

Fig. 1. Small-element model for transmission lines.

A schematic of a damaged segment and the traveling waves are shown in Fig. 2. The forward wave (incident wave) U_{f1} travels along the overhead line through a conductor with a characteristic impedance of Z_{c1}. When the incident wave reaches another medium with different characteristic impedance Z_{c2}, the wave is divided into forward and backward portions. The backward wave U_{r1} is calculated by multiplying U_{f1} by the reflection coefficient defined by (5), from [11]

$$r = \frac{(Z_{C2} - Z_{C1})}{(Z_{C2} + Z_{C1})} \tag{5}$$

where r is the reflection coefficient, and Z_{c1} and Z_{c2} are the characteristic impedances of two sections.

III. Power-Line Carriers

PLC systems and their peripheral equipment are used to communicate for the purpose of system protection, telemetry applications, and voice applications [7]. The coupling equipment consists of line tuners, coupling capacitors, drain coils, and line traps. According to [12], a drain coil must be provided in the coupling system, as shown in Fig. 2. The purpose of the drain coil is to provide a low-impedance path to the ground for the power frequency and, at the same time, to make a high-impedance path to the ground for the carrier frequency energy. The value of coupling capacitors must be selected based on Table II [7]. Frequencies in the range of 30–500 kHz can be generated by PLCs. This frequency range is sufficiently high to be isolated from the power frequency energy and the power system noise, but not high enough to encounter excessive attenuation [7] since the attenuation coefficient is in direct proportion to the frequency.

IV. Theoretical Models

In order to find flaws, appropriate models of components are used, and the simulations have been done using "EMTPWorks".

A. Conductors, Towers, Coupling Capacitors, and Drain Coils

In this work, the line model is the Constant Parameter (CP) model with the skin effect [13], and the ground relative resistivity is 100 ohm-meters. The transposing of long transmission lines increases the loss in comparison to non-transposed lines [7]. Therefore, lines are assumed fully transposed to make the situation worse. Each simulation has been done under its own frequency which is governed by the PLC.

Two geometrically distinct transmission lines are analyzed and the conductor type of each has been changed according to the general constraints. Tower details are shown in Figs. 3 and 4 from EMTP and [14], respectively. For the first tower configuration, the "Bluejay" and "Linnet" conductor types are appropriate, and for the second tower "Joree" and "Bluejay" types are suitable.

The circuit model used in the simulations is shown in Fig. 5. Both ends of the transmission line are considered open circuit

TABLE I
Specifications and Features of the Conductors Used in the Case Study

Conductor name	Stranding (Al/Stl)	Dia.Ind. Wire Al (Inches)	Dia.Ind. Wire Stl. (Inches)	Steel Core Diameter (Inches)	Cable Diameter (Inches)
Bluejay	45/7	0.1573	0.1049	0.3147	1.259
Joree	76/19	0.1819	0.0849	0.4245	1.880
Linnet	26/7	0.1137	0.0884	0.2642	0.720
Conductor name	% IACS Content – Al	% IACS Content – Stl	R_{DC} 20°C 1000ft. Measured.	R_{AC} 75°C 1000ft. Measured.	R_{DC} 75°C 1 km. Calc.
Bluejay	83.69	16.31	0.0155	0.0194	0.062855
Joree	86.73	13.27	0.0069	0.0094	0.027989
Linnet	68.53	31.47	0.0505	0.0618	0.204109

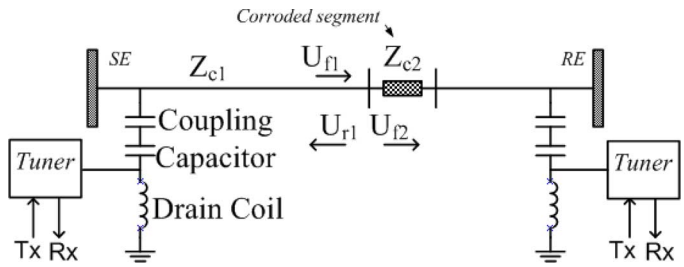

Fig. 2. Flawed section in the transmission line and PLC coupling apparatus circuit model.

TABLE II
Coupling Capacitor Value Based on Nominal Voltage

Voltage class (KV)	Capacitance range (uF)	Voltage class (KV)	Capacitance range (uF)
34	0.004 – 0.010	161	0.0012 – 0.014
46	0.004 – 0.015	230	0.0009 – 0.010
69	0.003 – 0.015	287	0.006 – 0.007
92	0.002 – 0.020	345	0.0005 – 0.006
115	0.0019 – 0.020	500	0.0014 – 0.005
138	0.0014 – 0.016	765	0.0023 – 0.005

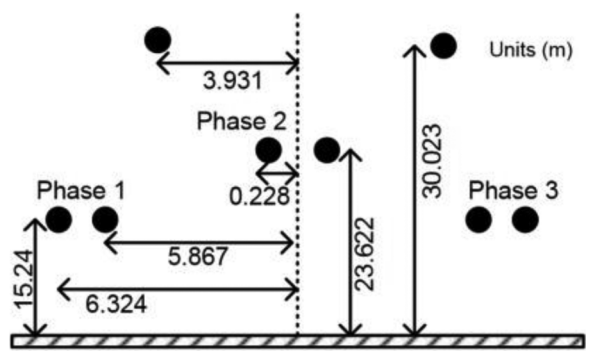

Fig. 3. Tower #1 geometrical specification, units are in meter.

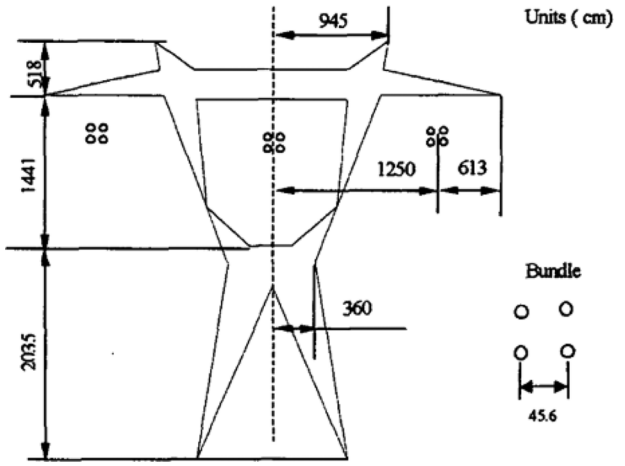

Fig. 4. Tower #2 geometrical specification, units are in centimeter.

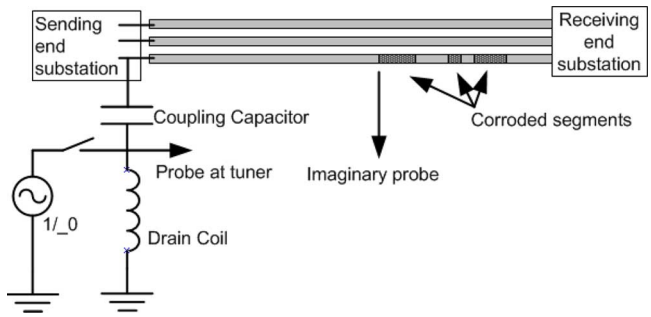

Fig. 5. Circuit model of tuner coupling and transmission line.

TABLE III
COUPLING ELEMENTS VALUES

Tower #1	230 KV	Coupling capacitance	Drain inductance	Resonance Freq.
		8 nF	0.3 mH	102 kHz.
Tower #2	765 KV	Coupling capacitance	Drain inductance	Resonance Freq.
		4 nF	0.5 mH	112 kHz.

at the PLC frequency because line traps are in series with the phases. Coupling capacitors are selected according to Table II. The value of the drain coil is chosen such that the resonance frequency is far from the PLC frequency [15]. The values which are used for simulations are presented in Table III.

B. Simulation Considerations

1) Conductor Temperature: The conductor temperature can reach 180°C [16], [17]. This high temperature increases the relative resistivity of the conductor. Therefore, the effect of temperature must be considered. The relation between temperature and relative resistivity is

$$\rho = \rho_0(1 + \alpha(T - T_0)) \tag{6}$$

where ρ_0 is the relative resistivity in the standard temperature (T_0), ρ is the relative resistivity in ambient temperature (T), and α is the linear temperature coefficient of the material.

Because of the reverse relation between temperature and skin depth, shown in Fig. 6, 75 °C is selected for simulations

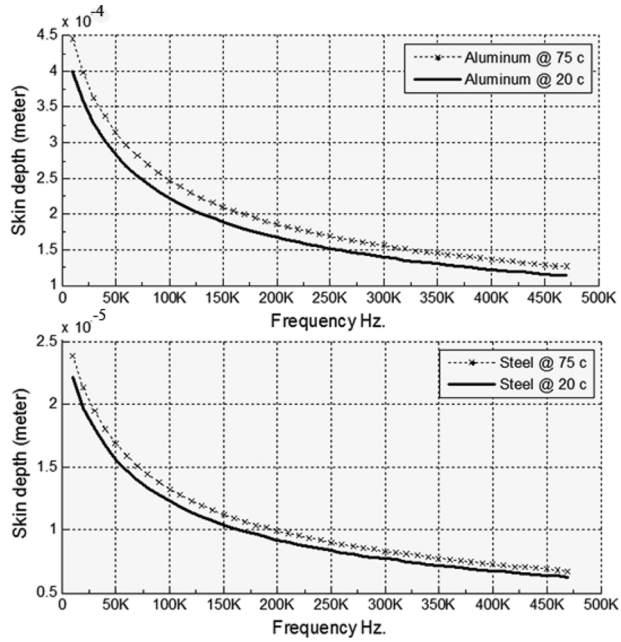

Fig. 6. Comparison of skin depth under normal ambient (20 °C) and common working temperature (75 °C).

as a common condition in transmission lines. Moreover, this temperature makes the situation worse to detect the defects. dc resistance at 75 °C has been calculated based on the specifications released by conductor manufacturers (mentioned in Table I, Calc. column).

2) Skin Effect: Almost 63% of ac current flows between the surface of a conductor and a level inside of it which is called skin depth and calculated by

$$\delta = \sqrt{\frac{2\rho}{(\mu\omega)}} \tag{7}$$

where δ is skin depth, μ and ρ are, the permeability and relative resistivity of the conductor, respectively.

For simulating the frequency-dependent behavior of conductors, the "Galloway and Wedepohl" and "T/D" methods are briefly described and compared in the following sub-sections.

"Galloway and Wedepohl" Method: Assuming that the depth of penetration is very small at high frequencies, the current density at the surface of the conductor is proportional to the magnetic-field intensity at the surface, as (8) shows [18].

$$Z_C = \frac{km\rho}{(r(n+2)\pi)} \tag{8}$$

where k is approximately equal to 2.25 due to conductor stranding, n is the number of strands in the outer layer, r is the radius of each outer strand, m is described with (9), and (10) is another expression of (8).

$$m = \sqrt{\frac{j\omega\mu}{\rho}} \tag{9}$$

$$R_{\mathrm{AC}} = X_{\mathrm{AC}} = \frac{km\rho}{(\sqrt{2}r(n+2)\pi)}. \tag{10}$$

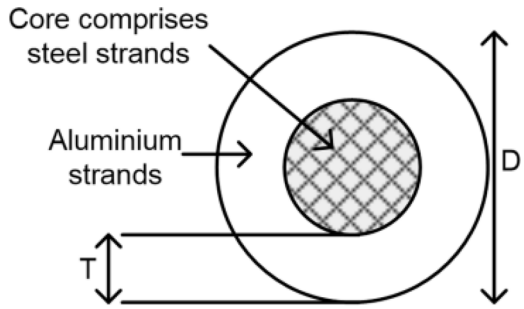

Fig. 7. T and D are marked on conductor cross-section.

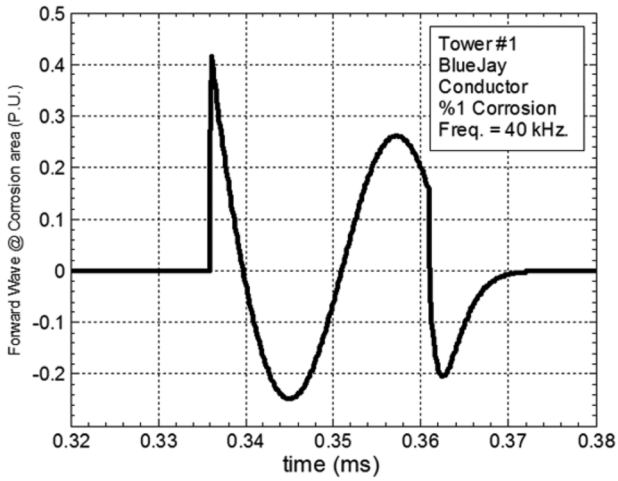

Fig. 8. Forward wave at the beginning of the damaged segment , sensed by an imaginary probe.

"T/D" Method: This method is based on the principle of the "Galloway-Wedepohl" method [19]. Equations (11)–(14) and the illustration, Fig. 7, are presented

$$k = 1 + 3.409 \times 10^{13} X^{2.078} Y^{3.92} - 3.32 \times 10^{-21} X^{4.55} Y^{Z} \tag{11}$$

$$X = \frac{T}{D} \tag{12}$$

$$Y = \sqrt{\frac{f}{R_{\mathrm{DC}}}} \tag{13}$$

$$Z = 6.50 - 1.27 X^{3.33}. \tag{14}$$

Comparison of the Methods: The "Galloway-Wedepohl" method is fairly proper for surface flaws, while the "T/D" method is appropriate for both internal and surface defects. Furthermore, the "T/D" model is more suitable for modeling the corroded and eroded areas. Thus, the "T/D" method was used in the simulations.

3) Electrical Parameters of Damaged Conductors: The damaged area on the cross-section is assumed as a percentage of the total diameter as shown in Tables V– VI, Fig. 19(a), and Fig. 19(b) in "Appendix". To provide an insight into corrosion patterns and their characteristics, some descriptions are stated in [20]–[22]. According to [23]–[25], the aluminum oxide resistivity grows to 10^{14} ohm.cm. Therefore, we assumed the flaws are empty of electrical current in comparison with the normal areas (Table I).

In order to calculate the impedance accurately when the defective area itself has an asymmetrical shape, numerical methods in frequency domain such as the Finite Integral Technique (FIT) [26] or the Finite Difference Frequency Domain (FDFD) [27] must be employed. For example, "CST" software can be a remedy [28]. The impedance of the un-uniformly damaged sections must be calculated in frequency domain, then the obtained values by (1)–(4) must be converted to Z_s, *Tau*, and R for "EMTPWorks".

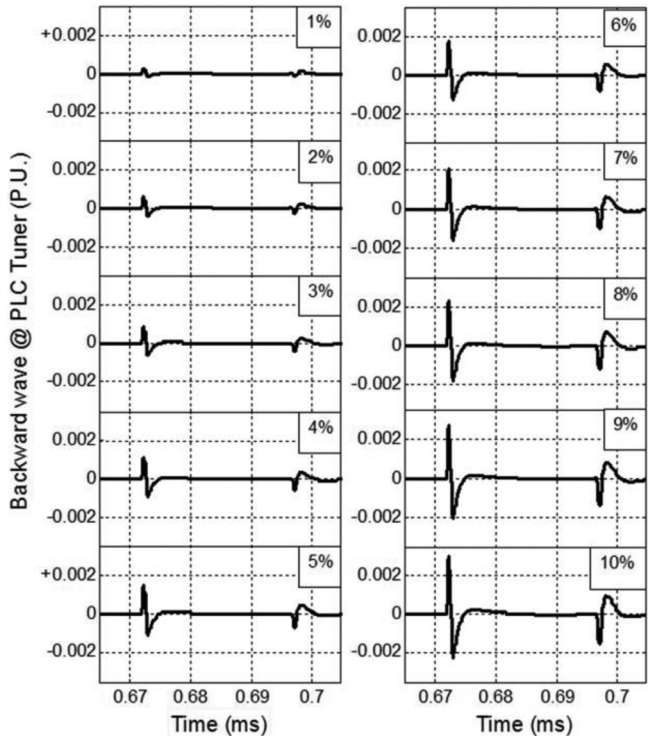

Fig. 9. Received wave at the location of the sending tuner, Tower #1, "Bluejay" conductor, PLC at 40 kHz, radius reductions are from 1% to 10%.

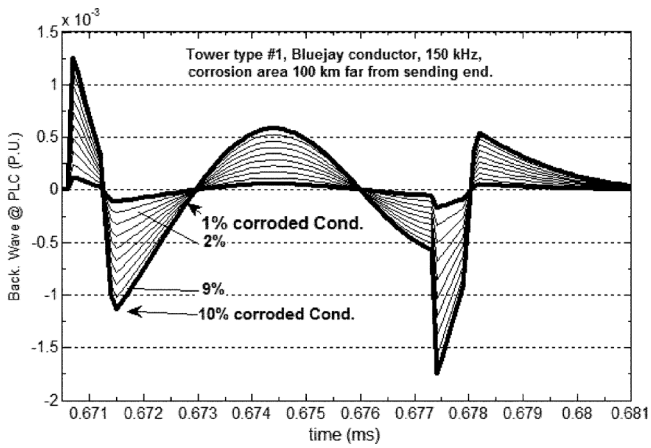

Fig. 10. Received wave at the tuner point for 1% to 10% radius reduction, Tower #1, "Bluejay" conductor, PLC at 150 kHz.

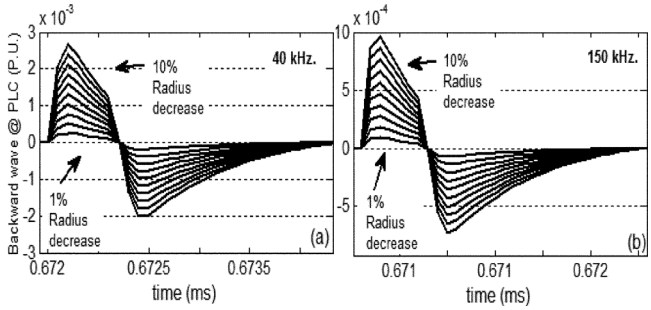

Fig. 11. Received signal at the sending end tuner, Tower #1, "Linnet" conductor. (a) Frequency of 40 kHz. (b) Frequency of 150 kHz.

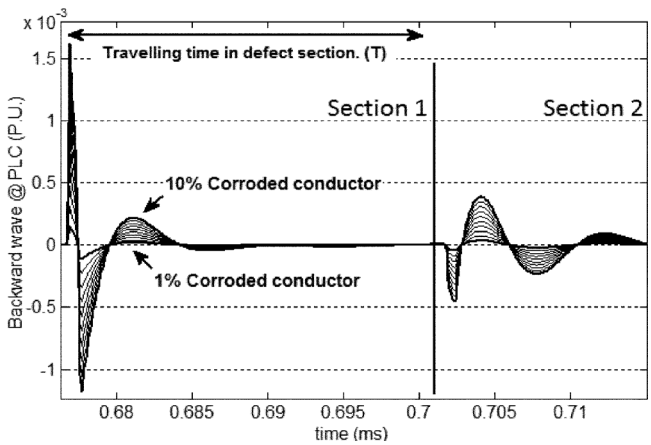

Fig. 12. Complete received wave from the beginning and the end of the defective section, Tower #2, "Bluejay" conductor, 40 kHz.

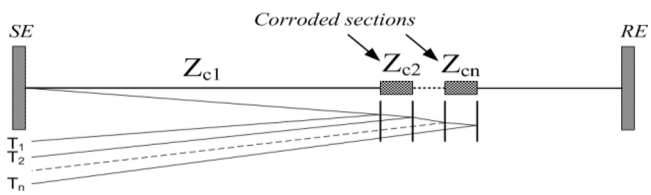

Fig. 13. Ladder curve of the forward and backward PLC signal in a transmission line. T_n is the n-th reflection time from the defects.

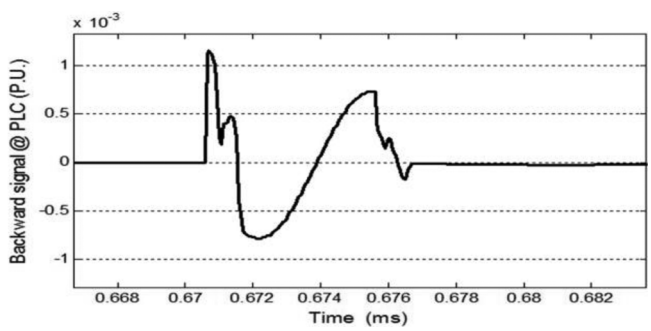

Fig. 14. Backward wave from four flaws in a power line. Tower #1, 150 kHz, "Bluejay". Four decays are: 50 (m), 6%; 20 (m), 2%; 30 (m), 4%; and 40 (m), 5%. The flaws are stuck to each other without any distance.

V. Simulation Results

The results of the simulation are presented in this section to explore the viability of the proposed method for detection of surface flaws.

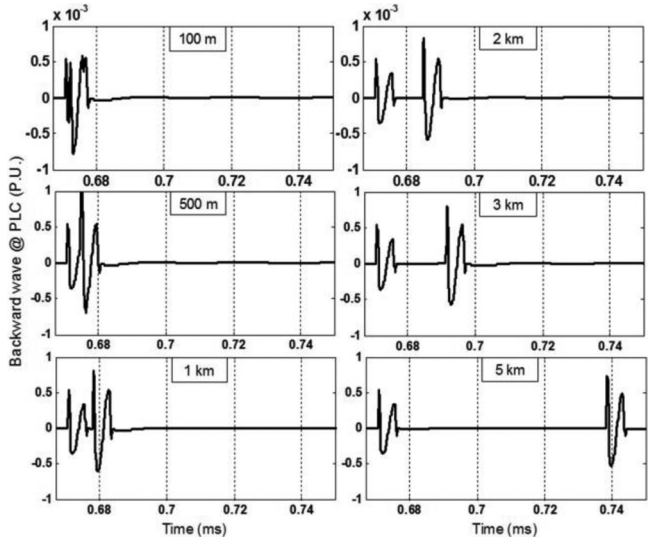

Fig. 15. Backward waves originated from two sequential flaws with variable distance from each other. The intermediate distance is noted on the curves. Tower #1, 150 kHz, 3% and 5% radius reduction.

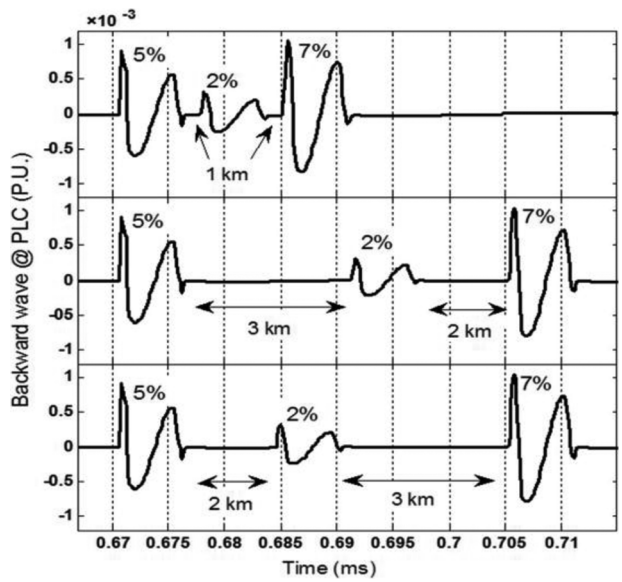

Fig. 16. Depiction of the reflections from three flaws. Tower #1, 150 kHz, "Bluejay," and each segment length is 100 meters.

A. Internal Corrosion

Internal corrosion leads to a minor change in conductor resistivity. Inductance is mainly dependent on the physical dimensions of the conductor and their topology on the tower. The dimensions of the conductor do not change by internal flaws. Therefore, the conductor resistance and inductance are approximately constant.

Characteristic impedances of intact and damaged (50% reduction, as a severe damage), "Bluejay" conductors are: $Z_s = 5.21582\text{E}+02$, R per length $= 5.70929\text{E}+01$; $Z_s = 5.21583\text{E}+02$, R per length $= 5.70949\text{E}+01$, respectively. Therefore, the reflection coefficient is in the order of 10^{-6}. This small reflection is prone to fade due to noise and the attenuation factor of the line. Consequently, the proposed method is not able to find internal flaws.

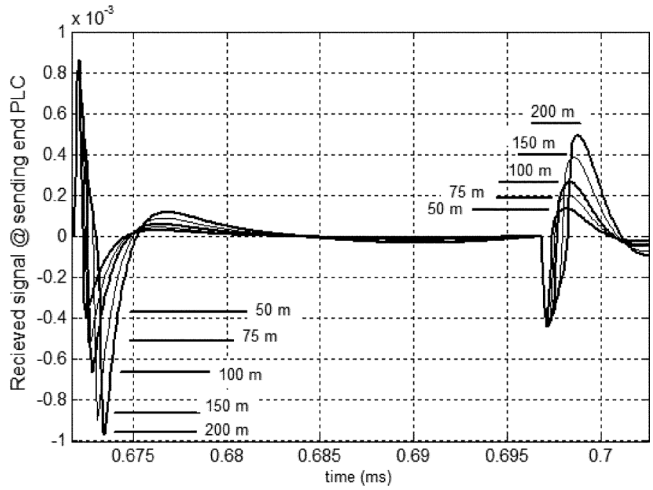

Fig. 17. Curves relating to the different defect lengths, Tower #1, 3% cross-section reduction, 40 kHz. Defect length is ranging from 50 to 200 meters.

TABLE IV
PEAK VALUE OF BACKWARD WAVES AT THE TUNER POINT FOR ALL SIMULATION CONDITIONS

	PLC Freq.	1%	2%	3%	4%	5%
Tower 1 Bluejay	40	-10.89	-4.83	-1.26	1.27	3.24
	150	-18.40	-12.32	-8.76	-6.21	-4.24
Tower 1 Linnet	40	-11.77	-5.72	-2.16	0.38	2.35
	150	-20.70	-14.65	-11.09	-8.55	-6.58
Tower 2 Bluejay	40	-16.18	-10.10	-6.55	-4	-2.03
	150	-27.18	-21.16	-17.58	-5.04	-13.06
Tower 2 Joree	40	-27.23	-11.94	-7.48	-4.95	-2.97
	150	-36.19	-20.1	-16.55	-14	-12.02
	PLC Freq.	6%	7%	8%	9%	10%
Tower 1 Bluejay	40	4.87	6.25	7.46	8.52	9.47
	150	-2.61	-1.23	-0.03	1.04	1.99
Tower 1 Linnet	40	3.98	5.36	6.56	7.62	8.59
	150	-4.95	-3.57	-2.37	-1.30	-0.35
Tower 2 Bluejay	40	-0.39	0.99	2.19	3.25	4.22
	150	-11.44	-10.05	-8.85	-7.78	-6.82
Tower 2 Joree	40	-1.34	0.04	1.24	0.31	3.27
	150	-10.39	-9.01	-7.81	-6.74	-5.78

Frequency is in kHz and the peak values are in dBm.
Note the equation, 'dBm = 20 log (mA)' is used.

B. Surface Decay

Surface damage reduces the effective cross-section, or diameter, of a conductor. Hence, the inductance of the flawed segment changes. If the area of surface defect and the area of internal defect are the same, the impedance of the externally corroded line is greater than that of the line which is internally corroded.

The Z_s of the damaged (1% reduction, as a minute damage), "Bluejay" conductor is: Zs $=$ 5.21890E $+$ 02 and R per length $=$ 5.70981E $+$ 01. Thus, as the results show, the reflection from the damaged section can be detected at the sending end. Therefore, the next simulations focus on surface defects.

Fig. 8 depicts the forward (incident) wave at the beginning of a damaged segment. This point is not accessible in practice, and the information derived from this point is not necessary for later estimations, but it can be used as a time reference for the following figures and also as an auxiliary point for examining the results shown in the following figures.

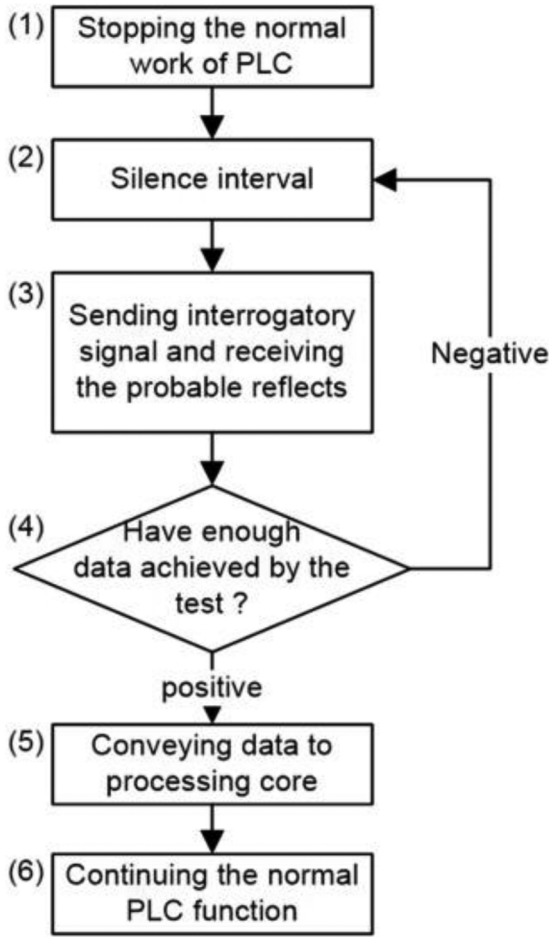

Fig. 18. Pattern of the sending signal.

Fig. 9 shows the reflected wave from the corroded section that is 100 km away from the PLC. The percentage of the radius reduction is shown in each diagram. This figure shows the relation between the severity of the damage and the amplitude of the received wave. Fig. 10 depicts some results similar to Fig. 9, but at a frequency of 150 kHz to show the effect of frequency on the attenuation factor and also the detectability of the defects under higher frequencies. Figs. 11(a) and 11(b) provide a comparative illustration between 40 and 150 kHz of frequency for the same condition.

Fig. 12 focuses on the full backward wave at the location of the tuner. Both reflections from the head and the end of the flaw are considered clearly.

VI. ESTIMATION AND EVALUATION

Travelling time is a useful parameter to estimate the distance, the length, and also the severity of the flawed segment. Thus, having an approximation of the velocity of the travelling wave is important.

A. Flaw Distance From the PLC Location

As Fig. 13 depicts, T_1 is the first reflection time from the flaw and its value is two times greater than the time shown in Fig. 8,

TABLE V
CONDUCTOR FEATURES' CORRECTION, ACCORDING TO INTERNAL CORROSION AT 75 °C

Conductor name		1%	5%	10%	20%	40%	50%
Bluejay	R_{DC} per km.	0.062956	0.063366	0.063903	0.065056	0.067719	0.069253
Joree	R_{DC} per km.	0.028024	0.028166	0.028353	0.028752	0.029670	0.030195
Linnet	R_{DC} per km.	0.204992	0.208636	0.213451	0.224054	0.250125	0.266346

TABLE VI
CONDUCTOR FEATURES' CORRECTION, ACCORDING TO SURFACE CORROSION AT 75 °C

Conductor name		1%	2%	3%	4%	5%
Bluejay	Diameter (cm)	3.1659	3.1339	3.1019	3.0699	3.0380
	R_{DC} per km.	0.064200	0.065588	0.067023	0.068506	0.070040
	T/D	0.374	0.372	0.371	0.370	0.368
Joree	Diameter (cm)	4.7274	4.6797	4.6319	4.5842	4.5364
	R_{DC} per km.	0.028583	0.029197	0.029830	0.030486	0.031163
	T/D	0.386	0.385	0.384	0.382	0.381
Linnet	Diameter (cm)	1.8105	1.7922	1.7739	1.7556	1.7374
	R_{DC} per km.	0.208567	0.213176	0.217944	0.222877	0.227985
	T/D	0.315	0.313	0.311	0.309	0.307
Conductor name		6%	7%	8%	9%	10%
Bluejay	Diameter (cm)	3.0060	2.9740	2.9420	2.9101	2.8781
	R_{DC} per km.	0.071628	0.073270	0.074971	0.076734	0.078560
	T/D	0.367	0.366	0.364	0.363	0.361
Joree	Diameter (cm)	4.4887	4.4409	4.3932	4.3454	4.2977
	R_{DC} per Km.	0.031863	0.032588	0.033338	0.034115	0.034920
	T/D	0.380	0.379	0.377	0.376	0.375
Linnet	Diameter (cm)	1.7191	1.7008	1.6825	1.6642	1.6459
	R_{DC} per Km.	0.233274	0.238755	0.244437	0.250329	0.256444
	T/D	0.305	0.303	0.301	0.298	0.296

therefore, the place where the corroded segment begins can be estimated by dividing T_1 by two times the wave propagation velocity in the medium (Distance $= T_1/2v$).

For the case of multiple flaws, if the distance between corroded segments is too short, as shown in Figs. 14 and 15 (100 meters and 500 meters), the decayed sections are seen as a long flaw. In other words, the reverse wave distorts. But if the corroded segments have enough distance from each other, according to Fig. 15 (1 km and more) and Fig. 16, they are separately detectable by the wave shape.

In practice, for either one defect or a number of close defects, the whole section of the conductor is replaced.

B. Flaw Length

The characteristics of the media are different at the beginning and the end of a defective segment. Therefore, two waves come back from the above mentioned points (as described by (5) and shown in Fig. 13). The left side of Fig. 12, Section I, shows the reflection from the beginning of the flaw. The right side of the figure Fig. 12, Section II, shows the reflection from the end of the flaw. The two waves are anti-phase (or have 180 ° phase difference). Fig. 17 shows the issue clearly. With reference to Fig. 13, the length of the corroded segment can be estimated by

$$L = \frac{T_n - T_{n-1}}{2 \times v} \tag{15}$$

where v is wave velocity (almost the velocity of wave in intact conductor), L is the length of the corroded section, and T_n and T_{n-1}, are the reflection times from the beginning and the end of the n-th defect, respectively.

As it is mentioned in the "Flaw Distance from PLC Location" section, if multiple corroded segments are close to each other, they are seen as a single section, but the backward waves from the beginning and the end of the whole section are still anti-phase, as (5) describes. Therefore, the overall length of the flawed section can be estimated. If the distance between the two neighboring flaws is long enough (Figs. 15 and 16), they can be seen as two separate corroded segments.

C. Defect Severity

From Fig. 9 to Fig. 12 and Table IV, it is obvious that the peak value of the received wave is reduced by the PLC operating frequency, the flaw distance from the PLC, the previous defects, and also any other changes in Z_s usually caused by a topological change of tower. The size of the backward wave at the beginning of a flaw can be estimated by cancelling out the effect of the cited factors. Thus, the range of the radius reduction of the conductor can be estimated.

If there are multiple sequential flaws, except for the first reflection from the beginning of the damaged part, the rest of the reflection shapes will be distorted, as Figs. 14 and 15 (100 and 500 meters) show. Therefore, there is no aggregate solution

for estimating the flaws, and the use of classification methods is necessary. The evaluation process must begin from the first segment because the backward wave reduces when it passes through the damaged segments. Hence, Z_c of the segments must be estimated from the beginning to the end of the line, successively.

D. Discussion About Using Classification Algorithms

According to the results shown in Figs. 14 and 15, regular and irregular patterns of the backward waves can be a trace for distinguishing the entity of the flawed segment. Although it is enough to have a rough estimation of the conductor condition, the irregular waveforms should be checked to achieve a more accurate evaluation. It is worth noting that most parameter identification problems inherently do not have a unique answer. In the case of multiple flaws, the use of intelligent identification/classification algorithms, such as the neural network or the fuzzy logic, can be a remedy.

VII. Signaling Procedure

The entity of the interrogatory signal is a plain sine wave. It has been selected based on the PLC capability and the fact that a single frequency wave is simpler to deal with. There are two types of carrier operations: Frequency Shift Keying (FSK), and On-Off carrier. In the FSK operation mode, the sending wave can be keyed from a far frequency to the desired one for conductor diagnosing. In the case of On-Off carrier, the sending signal is able to be on or off. Both carriers can be employed with a predictable and changeable duty cycle. A flowchart of the PLC signaling for NDT purposes is shown in Fig. 18. The important parts in this flowchart are described below.

A. Stopping the Normal PLC Work

At first, the PLC stops working. The receiver side must be informed to prevent misunderstandings such as protection system malfunction.

B. Silence Interval

By accommodating a silent gap before sending the interrogatory wave, two goals are achieved: 1) Depleting the channel from the remains of the normal PLC signals which may interfere with the NDT processes. 2) Evaluating the channel noise. With the information obtained about the channel noise, more effective noise reduction measures can be used.

C. Sending Interrogatory Signal and Receiving Reflections

The test procedure continues with sending the forward signal in pulse form. The probable reflections from the flaws are detected in this step. This section and section two must be repeated until enough data are collected for the selected parameter estimation method and noise reduction algorithm.

VIII. Practical Aspects

In practice, there are a number of parameters that could affect the performance of the proposed method. These include noise consideration, reflections from discontinuities other than defects, and the weather condition [7].

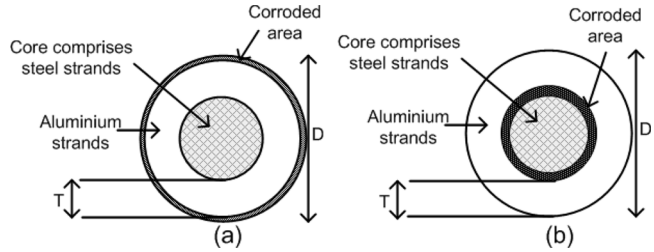

Fig. 19. (a) Surface and (b) internal corrosion in terms of T and D reduction.

A. Noise Consideration

The peak values of the reflected waves are given in Table IV. The noise level of power lines is approximately from -40 dBm at 350 kHz under fair weather to 0 dBm at 40 kHz under adverse weather [7]. Considering the data given in Table IV, the Signal to Noise Ratio (SNR) is adequate for detecting the flaws.

B. Reflections From Discontinuities Other Than Defects

Short discontinuities, like splices and tap points, cause unwanted reflections which are very sharp in shape; therefore, the frequency content of them is so high that they can be removed by reducing the sampling rate. Long discontinuities, like transitions and different topologies, produce reflections similar to damaged segments; however, having the power-line plan, we can predict such backward waves, or spurious reflections, in terms of both size and location.

C. Weather Condition

Volatility in ambient is unavoidable, but testing the conductor could be confined to the most proper weather.

IX. Conclusion

A non-destructive testing technique has been introduced to detect corrosion/erosion defects on the surface of phase conductors along a power transmission line. The technique which uses the elements of PLCs is based on the backward-wave propagation produced by a change in the characteristic impedance of a power transmission line, resulting from corrosion or erosion.

The method introduced in this paper not only exempts the need for close following the line route, but can also be used with the existing apparatus. External and internal flaws are studied, and the new method is shown by simulations to be able to detect and evaluate surface defects. These defects can be either single or multiple in any phase, in spite of the condition of the other phases. Physical/field tests under the real world conditions to verify and amend the setting of the proposed method are necessary.

Appendix

The simulations for internal and superficial flaws are performed according to the detailed specifications of the conductors shown in Tables V and VI. The assumptions made for estimating the flaws on the cross-section of conductors are shown in Fig. 19.

References

[1] *Corrosion of Metals and Alloys -Corrosivity of Atmospheres—Classification*, ISO 9223:1992.

[2] *Corrosion of Metals and Alloys -Corrosivity of Atmospheres—Guiding Values for the Corrosivity Categories*, ISO 9224:1992.
[3] G. Chen, X. Wangb, J. Wanga, J. Liu, T. Zhang, and W. Tang, "Damage investigation of the aged aluminum cable steel reinforced (ACSR) conductors in a high-voltage transmission line," in *Eng. Failure Anal.*, Sep. 2011, pp. 13–21.
[4] D. G. Harvard, G. Bellamy, P. G. Buchan, Ewing, H. A. Horrocks, D. J. Krishnasamy, S. G. Motlis, and J. Yoshiki-Gravelsins, "Aged ACSR conductors. I. testing procedures for conductors and line items," *IEEE Trans. Power Del.*, vol. 7, no. 2, pp. 581–587, Apr. 1992.
[5] Agency of Department of Energy, Office of Federal Locations, Solicitation Number: DE-FB75–11WG91874. [Online]. Available: https://www.fbo.gov/
[6] J. Sutton and K. G. Lewis, "The detection of internal corrosion in steel-reinforced aluminum overhead power line conductors," in *Proc. UK Corrosion*, Birmingham, U.K., 1987, vol. 1, pp. 345–359.
[7] *IEEE Guide for Power-Line Carrier Applications*, IEEE Standard 643–2004, IEEE Power Eng. Soc.
[8] A. V. Pinto Jr, M. Z. Sebro, C. Regina, S. H. Lourenco, I. S. d. Almeida, J. Saad Jr, and P. M. Lourenco, "Remote detection of internal corrosion in conductor cables of power transmission lines," presented at the Int. Conf. Appl. Robot. Power Ind., Montréal, QC, Canada, Oct. 5–7, 2010.
[9] "Helicopter flights for the inspection, repair or maintenance of overhead electricity power lines," Irish Aviation Authority, Safety Regulation Division, NR O.64, no. 1, 2012.
[10] S. Hrabar, T. Merz, and D. Frousheger, "Development of an autonomous helicopter for aerial powerline inspections," presented at the 1st Int. Conf. Appl. Robot. Power Ind. Delta Centre-Ville, Montréal, QC, Canada, Oct. 5–7, 2010.
[11] L. v. d. Sluis, *Transients in Power Systems*. New York: Wiley, 2001.
[12] *Requirements for Power-Line Coupling Capacitors and Coupling Capacitor Voltage Transformers (CCVT)*, ANSI Standard C93.2, American National Standards Institute .
[13] *Electromagnetic Transient Program Theory Book*. Portland, OR, USA: Bonneville Power Administration, 1987.
[14] W. Que and S. A. Sebo, "Electric field and potential distributions along dry and clean non-ceramic insulators," in *Proc. IEEE Elect. Insul. Elect. Manuf. Oil Winding Conf.*, 2001, pp. 441–444.
[15] *IndustrialIT for Utility Communications*. Baden, Switzerland: ABB Switzerland Ltd., 2000.
[16] *IEEE Standard for Calculating the Current-Temperature of Bare Overhead Conductors*, IEEE Standard 738–1993, IEEE Power Eng. Soc..
[17] V. T. Morgan, "Effects of alternating and direct current, power frequency, temperature, and tension on the electrical parameters of ACSR conductors," *IEEE Trans. Power Del.*, vol. 18, no. 3, pp. 859–866, Jul. 2003.
[18] R. H. Galloway, W. B. Shorrocks, and L. M. Wedepohl, "Calculation of electrical parameters for short and long polyphase transmission lines," *Proc. Inst. Elect. Eng.*, vol. I11, no. 12, Dec. 1974.
[19] V. T. Morgan, R. D. Findlay, and S. Derrah, "New formula to calculate the skin effect in isolated tubular conductors at low frequencies," *Proc. Inst. Elect. Eng., Sci. Meas. Technol.*, vol. 147, no. 4, Jul. 2000.
[20] J. Calittz, "Overhead conductor corrosion study," M.Sc. dissertation, Dept. Chem. Metall. l Eng., Tshwane Univ. of Technology, Pretoria West, South Africa, 2004.
[21] S.-D. Kim and M. M. Morcos, "Mechanical deterioration of ACSR conductors due to forest fires," *IEEE Trans. Power Del.*, vol. 18, no. 1, pp. 271–276, Jan. 2003.
[22] E. W. Greenfield and E. W. Everhart, "A field study of ACSR cable in severe marine and industrial environment," *Power App. Syst., Part III. Trans. Amer. Inst. Elect. Eng.*, pp. 106–117, 1957.
[23] *Materials Science and Engineering Handbook*, J. F. Shackelford and W. Alexander, Eds. Boca Raton, FL, USA: CRC, 2001.
[24] G. Elert, *The Physics Hypertextbook*. Brooklyn, NY, USA: Midwood Science. [Online]. Available: http://physics.info/electric-resistance/
[25] K. Habib, "Measurement of surface resistivity/conductivity of anodized aluminum alloy by optical interferometry techniques," presented at the SPIE 7649, Nondestruct. Characteriz. Composite Mater., Aerosp. Eng., Civil Infrastruct., Homeland Security San Diego, CA, USA, 2010.
[26] T. Weiland, "A discretization method for the solution of maxwell's equations for six-component fields," *Electron. Commun. AEUE*, vol. 31, no. 3, pp. 116–120, 1977.
[27] A. Christ and H. L. Hartnagel, "Three-dimensional finite-difference method for the analysis of microwave-device embedding," *IEEE Trans. Microw. Theory Tech.*, vol. MTT-35, no. 8, pp. 688–696, Aug. 1987.
[28] CST Studio Suite Version 2014 - Update Webinar Series. CST-Computer Simulation Technology, Darmstadt, Germany, 2014. [Online]. Available: http://www.cst.com/.

R. Jalilzadeh Hamidi (S'13), photograph and biography not available at the time of publication.

Seyed Hossein Hosseinian, photograph and biography not available at the time of publication.

Seyed Hossein Hesamedin Sadeghi (M'92–SM'05), photograph and biography not available at the time of publication.

Zhihua Qu (F'10), photograph and biography not available at the time of publication.